AUT Journal of Modeling and Simulation

AUT J. Model. Simul., 54(1) (2022) 31-44
DOI: 10.22060/miscj.2022.21010.5268

Transfer Alignment Configuration Based on Angular Velocity and Angular Velocity Integral Applied to Marine Vehicles

M. Amuei[1], S. M. Mehdi Dehghan[1*], H. Nourmohammadi[2], M. A. AlirezaPouri[2]

[1]-Faculty of Electrical and Computer Engineering, Malek-Ashtar University of technology, Tehran, Iran
[2]-Northern Reasearch Center for Science and Technology, Malek-Ashtar University of technology, Fereydunkenar, Mazandaran

ABSTRACT: Transfer alignment of master and slave systems plays a key role in the inertial navigation accuracy of the marine cooperative vehicles. Accuracy enhancement of misalignment angle and orientation estimation is the main purpose of the transfer alignment. Velocity and orientation matching is a well-known method for transfer alignment. However, in many applications, there are no velocity measurements of both the master and slave systems due to weight, dimensional and technological limitations of accurate speed sensors, such as Doppler Velocity Loggers (DVL). Angular velocity configuration is a suitable solution for transfer alignment in this situation. However, the orientation error cannot be estimated in this configuration. Taking this drawback into account, a new configuration based on using the integral of angular velocity in addition to angular velocity measurement is presented for transfer alignment in the current research. Furthermore, appropriate abilities are considered to estimate the dynamic misalignment angle, orientation error and also measurement errors of the slave gyroscope. Two linear and non-linear observation models are developed for the transfer alignment configuration. The simulation results reveal the appropriate performance of the proposed configuration for marine application, especially when there are no accurate velocity measurements. Based on the simulation results, the performance of the non-linear observation model is better than linear ones in dynamic misalignment angle estimation. Moreover, it can be inferred from the orientation error estimation that rich data in high-maneuvered motion is necessary for required estimation accuracy. Additionally, 200 runs of Monte-Carlo simulation are developed and the estimation RMSE are presented.

Review History:

Received: Jan. 20, 2022
Revised: Aug. 20, 2022
Accepted: Aug. 22, 2022
Available Online: Oct. 01, 2022

Keywords:

Transfer alignment
angular velocity matching
integral angular velocity matching
Kalman filter
misalignment angle

1- Introduction

Due to substantial restrictions of radio or satellite navigation, Inertial Navigation System (INS) is the main approach for marine navigation. However, alignment and calibration procedure are the main challenges of using the INS in marine applications. There are several methods to align the slave INS. Transfer alignment with velocity and orientation configuration is conventional for this purpose. This method uses the difference of velocity and orientation between the slave and master system for transfer alignment. The main challenge arises when velocity and orientation measurements of the slave or the master and slave systems do not exist. In these conditions, suitable measurements must be used for misalignment angle and orientation error estimation. Difference of angular velocity measurement is an appropriate configuration in order to estimate the misalignment angle and the slave gyroscope bias. However, the orientation error cannot be estimated in this configuration. Therefore, in the current research work, the integral of the angular velocity measurements are augmented to the angular velocity measurement for orientation error estimation.

There are some researches which use angular velocity measurement in transfer alignment configuration. In [1] a transfer alignment algorithm has been designed based on angular velocity configuration and H_∞ state estimation filter. The dynamic misalignment angle data is generated by second-order, third-order and fourth-order Markov process. Afterwards, H_∞ and Kalman filters are separately applied to estimate the misalignment angle. Simulation results indicate the H_∞ filter is more precise under sea disturbance. Song et al. compared the performance of Kalman filter and H_∞ filter in the transfer alignment problem, at the point of the environment noise [2]. The Kalman filter is more accurate compared to H_∞ filter when system noise and measurement noise are white noise. However, the H_∞ filter has a better performance in the conditions of colored noises. The angular velocity matching method for the transfer alignment on a moving platform has also been investigated in [3]. In this research, the effects of substantial factors and filter parameters in the estimation accuracy and the convergence speed of the state-estimation filter have been studied. In [4], a sea transfer alignment algorithm is designed, and usual Kalman filter is used for misalignment angle and gyroscope bias estimation. Simulation results indicate that slave system transfer alignment is satisfied in sea condition. In some researches,

*Corresponding author's email: smmd@mut.ac.ir

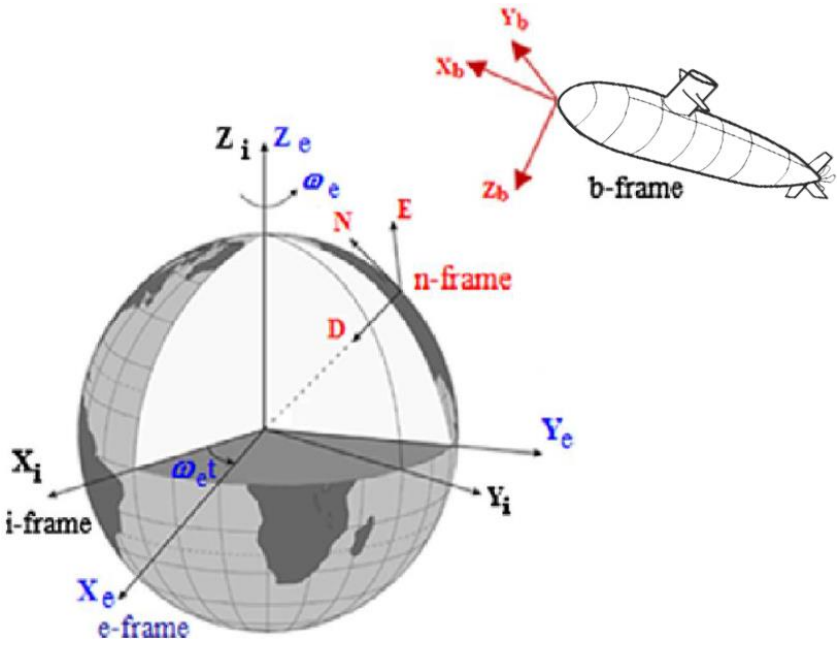

Fig. 1. Reference frames in the inertial navigation

extra-misalignment angle and gyroscope bias errors are also estimated. For example, in [5], transfer alignment with orientation plus velocity matching and orientation plus angular velocity matching have been compared in circumstance of sea waves and parameters of dynamic deformation of ships. Simulation results show that orientation plus angular velocity matching leads to superior accuracy of misalignment estimation. Moreover, Geng et al. investigated the lever arm effect in transfer alignment and orientation estimation error, velocity error, misalignment angle and gyroscope bias [6]. Cao et al. developed a new algorithm for position error estimation from velocity and angular velocity measurements [7]. In [8], velocity plus angular velocity configuration was applied in the implementation of the transfer alignment. Simulation results indicate that this method can accurately accomplish the alignment of a mooring weapon INS of the ship with large heading error. In [9], orientation error and gyroscope bias have been estimated using federated and fuzzy adaptive filter. A transfer alignment method of strap-down Inertial Navigation System on a moving platform based on combined parameter matching methods is introduced in [10]. In [11], an adaptive transfer alignment method based on the observability analysis for the strapdown Inertial Navigation System was proposed. In this research, according to the weight of the observability, a transfer alignment filter algorithm based on adaptive adjustment factor was constructed to reduce the influence of weak observability state variables on the whole filter due to acceptable observability of all states. This research uses attitude and velocity configuration for transfer alignment. However, due to lake of basic requirements for attitude configuration, we use just use angular velocity and angular velocity integral configuration for transfer alignment in the proposed scheme. In [12], those techniques that can be applied in the presence of elastic motion of aircraft wing were analyzed. This research investigated several configurations for transfer alignment such as acceleration/rotation rate, velocity, integral velocity and attitude, and velocity configuration. Due to practical and conceptual restrictions, we use a new configuration for transfer alignment. In [13], a decoupling method for the airborne dynamic deformation angle was proposed. This research used angular velocity, attitude and velocity configuration, and focused on decoupling dynamic misalignment angle problem, while in our work, the deformation of the floating boats and underwater vehicles of the ship is small. Despite of valuable researches accomplished in the previous works, there is no research that uses angular velocity and integral of angular velocity measurement to estimate misalignment angle, orientation error, and gyroscope bias at sea disturbed conditions. As the main advantage, the proposed configuration does not need additional measurements, such as velocity, position, and orientation measurements. In other words, this paper wants to solve the alignment problem in conditions that expensive and heavy DVL velocity instruments do not exist. This approach is suitable for disturbed conditions at sea where the initial navigation data are not available. Additionally, it can be used for alignment and calibration of many kinds of Inertial Navigation System and Attitude-Heading Reference System. Some applications of this research are transfer alignment of the floating boats and underwater vehicles of the ship.

2- Problem Statement

In this section, the concept of the transfer alignment is described. First, we introduce the reference frames used in the text, including inertial frame, earth frame, navigation frame, and body frame, as illustrated in Fig. 1 [14].

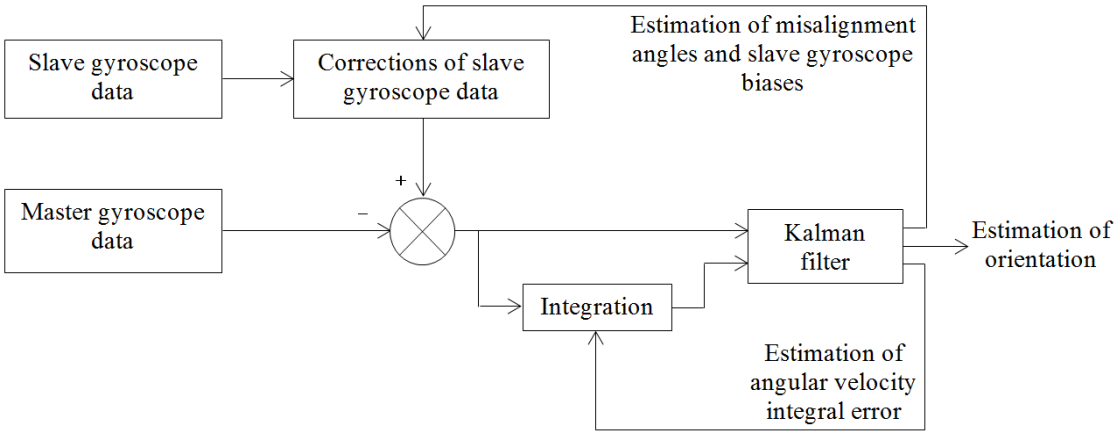

Fig. 2. Block diagram of the proposed transfer alignment configuration

Here, the purpose is transfer alignment of slave system based on the difference of the angular velocity and angular velocity integral measurements between the slave and master vehicles. The cost and accuracy of the sensors and equipment in the slave vehicle is less than those of the master vehicle. Transfer alignment of the slave system needs reference data provided from the master system [15]. The ultimate purpose of the transfer alignment is to estimate misalignment angle, orientation error, and also gyroscope bias of the slave system. In this work, we consider static misalignment angles as a part of orientation error. Dynamic misalignment angles between body axes of the slave and the master systems vary with time. The orientation error is the frame angular error between the real and erroneous axes of the slave coordinate frame. Transfer alignment configuration refers to the main measurements that are used in the transfer alignment. Configuration algorithms of the transfer alignment are often categorized in two classes [2], as follows.

- Calculated parameter matching, such as velocity and attitude matching
- Measuring parameter matching, such as acceleration and angular velocity matching

In marine applications, there are no velocity, position, and orientation measurements of both the master and slave systems due to weight, dimensional, and technological limitations of marine sensors. Accordingly, the difference of angular velocity and angular velocity integral of the slave and master systems are considered in the proposed transfer alignment configuration, as shown in Fig. 2.

As shown in Fig. 2, first, the error between the corrected slave gyroscope and the master gyroscope outputs are integrated. Next, difference of the angular velocity and the angular velocity integral are used in Kalman filter. Accordingly, misalignment angle, orientation error, slave gyroscope bias, and integral of angular velocity error are estimated. The estimated misalignment angle and the slave gyroscope bias are used to correct the slave gyroscope data. Additionally, the estimated angular velocity integral error is used as initial condition for integration and this procedure does, iteratively. The main contributions of the paper can be summarized as follows:

- Developing a new configuration for transfer alignment by using angular velocity integral
- Estimation of orientation error where there are no measurements for position and velocity
- Developing an applied algorithm for low-cost transfer alignment system in marine applications

3- System Dynamic

This section presents the system model, including dynamic misalignment angles model, gyroscope bias model, orientation error, and angular velocity integral error model.

3- 1- Dynamic Misalignment Angle Model

All dynamic misalignment angles (θ_i) along x, y, and z-axis are supposed to be a second-order Markov process, which can be described as follows [16]:

$$\ddot{\theta}_i + 2\beta_i\dot{\theta}_i + \beta_i^2\theta_i = \eta_i \quad (i = x, y, z) \tag{1}$$

In which, η_i is the Gaussian white noise sequence with variance Q_i. β_i and Q_i are considered as follows:

$$\begin{aligned} Q_i &= 4\beta_i^3\sigma_i^2 \quad (i = x, y, z) \\ \beta_i &= 2.146/\tau_i \quad (i = x, y, z) \end{aligned} , \tag{2}$$

where τ_i denotes the correlation time of the random process, and σ_i^2 represents the variance of the associated angle.

3- 2- Gyroscope Bias Model

The gyroscope biases are supposed to be time-constant. Therefore, the gyroscope biases can be mathematically modeled by zero dynamics [17]:

$$\dot{\boldsymbol{\varepsilon}} = \boldsymbol{w}_{\varepsilon} \quad , \quad \boldsymbol{w}_{\varepsilon} \sim N(0, \boldsymbol{B}) \quad ,$$
$$\boldsymbol{B} = \begin{bmatrix} B_x & 0 & 0 \\ 0 & B_y & 0 \\ 0 & 0 & B_z \end{bmatrix} \tag{3}$$

Where, $\boldsymbol{\varepsilon} = \begin{bmatrix} \varepsilon_x & \varepsilon_y & \varepsilon_z \end{bmatrix}^T$ stands for the gyroscope bias vector, and $\boldsymbol{B}$ is the covariance matrix of the gyroscope bias.

$$\delta\dot{\boldsymbol{\varphi}} = -\boldsymbol{\omega}_{in}^{n} \times \delta\boldsymbol{\varphi} + \delta\boldsymbol{\omega}_{in}^{n} + \boldsymbol{C}_b^n \boldsymbol{\varepsilon} + \boldsymbol{w}_{\delta\boldsymbol{\varphi}} \quad ,$$
$$\boldsymbol{w}_{\delta\boldsymbol{\varphi}} \sim N(0, \boldsymbol{A}) \quad , \quad \boldsymbol{A} = \begin{bmatrix} A_N & 0 & 0 \\ 0 & A_E & 0 \\ 0 & 0 & A_D \end{bmatrix} \tag{4}$$

3- 3- Orientation Error Model and Angular Velocity Integral Error Model

The Orientation error can be modeled as [18]:

where, $\delta\boldsymbol{\varphi} = [\delta\varphi_N \quad \delta\varphi_E \quad \delta\varphi_D]^T$ denotes orientation errors vector and $\delta\varphi_N$, $\delta\varphi_E$ and $\delta\varphi_D$ are orientation error along North-axis, East-axis and Down-axis of navigation frame, respectively. $\boldsymbol{\omega}_{in}^{n}$ is the angular velocity vector of the navigation frame with respect to the inertial frame, and $\delta\boldsymbol{\omega}_{in}^{n}$ is its error. $\boldsymbol{C}_b^n$ is direction cosine matrix from body to navigation frame [19], and A_N, A_E and A_D are the variance of the orientation error around North, East and Down-axis, respectively.

Angular velocity integral error can be modeled as [20]:

$$\dot{\boldsymbol{IW}} = \left[\boldsymbol{\omega}_{im}^{n} \times\right] \delta\boldsymbol{\varphi} + \boldsymbol{C}_b^n \boldsymbol{\varepsilon} + \boldsymbol{w}_{IW} \quad ,$$
$$\boldsymbol{w}_{IW} \sim N(0, \boldsymbol{G}) \quad , \quad \boldsymbol{G} = \begin{bmatrix} G_N & 0 & 0 \\ 0 & G_E & 0 \\ 0 & 0 & G_D \end{bmatrix} \tag{5}$$

In (6), $\boldsymbol{IW} = [\, IW_N \quad IW_E \quad IW_D \,]$ stands for the integral of angular velocity errors vector and IW_N, IW_E and IW_D are its components along North-axis, East-axis and Down-axis of the navigation frame, respectively. $\boldsymbol{\omega}_{im}^{n}$ is the angular velocity vector of master system with respect to inertial frame, and G_N, G_E and G_D are the variance of the integral of angular velocity error around North, East and Down-axis, respectively.

Finally, the state vector is constituted by dynamic misalignment angles, first-order derivative of the dynamic misalignment angles, gyroscope biases, orientation errors and integral of angular velocity errors as follows.

$$\boldsymbol{X}_{15\times1} = \begin{bmatrix} \theta_x & \theta_y & \theta_z & \dot{\theta}_x & \dot{\theta}_y & \dot{\theta}_z & \varepsilon_x & \varepsilon_y & \varepsilon_z \\ \delta\varphi_N & \delta\varphi_E & \delta\varphi_D & IW_N & IW_E & IW_D \end{bmatrix}^T \tag{6}$$

4- Measurement System

As referred in section 2, transfer alignment accomplishes with angular velocity and angular velocity integral measurements. In other words, the observation of the estimation process is constituted based on the difference of angular velocity and angular integral velocity between the slave and master vehicles.

4- 1- . Angular Velocity Configuration

In the angular velocity configuration, two linear and nonlinear models are used in the measurement systems, which are separately described in the following sections.

4- 1- 1- Linear Model

In the linear model, the transformation matrix between the slave and master body frames can be written as:

$$\boldsymbol{C}_M^S = \begin{bmatrix} 1 & \theta_z & -\theta_y \\ -\theta_z & 1 & \theta_x \\ \theta_y & -\theta_x & 1 \end{bmatrix} \tag{7}$$

Eq. (7) can be rewritten as:

$$\boldsymbol{C}_M^S = \boldsymbol{I}_{3\times3} - [\boldsymbol{\theta}\times] \tag{8}$$

In (8), $[\boldsymbol{\theta}\times]$ is the skew symmetric matrix of $\boldsymbol{\theta}$ vector. Considering (9) and derivation of dynamic misalignment angle and gyroscope bias, the relationship between outputs of the slave and master gyroscopes can be explained as:

$$\boldsymbol{\omega}_{ib}^{S} = \left(\boldsymbol{I}_{3\times3} - [\boldsymbol{\theta}\times]\right)\boldsymbol{\omega}_{ib}^{M} + \dot{\boldsymbol{\theta}} + \boldsymbol{\varepsilon} \tag{9}$$

Where, $\boldsymbol{\omega}_{ib}^{S}$ and $\boldsymbol{\omega}_{ib}^{M}$ are the output of the slave and the master gyroscopes, respectively. Eq. (9) can be rewritten as:

$$\boldsymbol{\omega}_{ib}^{S} - \boldsymbol{\omega}_{ib}^{M} = \left[\boldsymbol{\omega}_{ib}^{M} \times\right]\boldsymbol{\theta} + \dot{\boldsymbol{\theta}} + \boldsymbol{\varepsilon} \tag{10}$$

In (10), $[\boldsymbol{\omega}_{ib}^{M}\times]$ is the skew symmetric matrix of $\boldsymbol{\omega}_{ib}^{M}$. Accordingly, the linear model of the angular velocity observation can be written as:

$$\boldsymbol{Z}_{\omega}=\left[\boldsymbol{\omega}_{ib}^{M}\times\right]\boldsymbol{\theta}+\dot{\boldsymbol{\theta}}+\boldsymbol{\varepsilon}+\boldsymbol{v}_{\omega}\quad,$$

$$\boldsymbol{v}_{\omega}\sim N(0,\boldsymbol{O})\quad,\quad \boldsymbol{O}=\begin{bmatrix}O_x & 0 & 0\\ 0 & O_y & 0\\ 0 & 0 & O_z\end{bmatrix} \tag{11}$$

where, $\boldsymbol{Z}_{w}$ is the angular velocity measurement vector, and $\boldsymbol{O}$ is the covariance matrix of the angular velocity measurement model.

4- 1- 2- Nonlinear Model

In the nonlinear model, the relationship between outputs of the slave and master gyroscopes can be explained as follows [16].

$$\boldsymbol{\omega}_{ib}^{S}=\boldsymbol{C}(\boldsymbol{\theta})\boldsymbol{\omega}_{ib}^{M}+\boldsymbol{\omega}_{MS}^{S} \tag{12}$$

where, $\boldsymbol{\omega}_{MS}^{S}$ represents the relative angular velocity between the master and the slave system. **C(θ)** is rotation matrix of dynamic misalignment angles. The rotation order x → y → z is chosen and **C(θ)** is given by:

$$\boldsymbol{C}(\boldsymbol{\theta})=\boldsymbol{C}(\theta_z)\boldsymbol{C}(\theta_y)\boldsymbol{C}(\theta_x) \tag{13}$$

where, $\boldsymbol{C}(\theta_x)$, $\boldsymbol{C}(\theta_y)$ and $\boldsymbol{C}(\theta_z)$ are defined as follows.

$$\boldsymbol{C}(\theta_x)=\begin{bmatrix}1 & 0 & 0\\ 0 & cos\theta_x & sin\theta_x\\ 0 & -sin\theta_x & cos\theta_x\end{bmatrix}\quad,\quad \boldsymbol{C}(\theta_y)=\begin{bmatrix}cos\theta_y & 0 & -sin\theta_y\\ 0 & 1 & 0\\ sin\theta_y & 0 & cos\theta_y\end{bmatrix}\quad,$$
$$\boldsymbol{C}(\theta_z)=\begin{bmatrix}cos\theta_z & sin\theta_z & 0\\ -sin\theta_z & cos\theta_z & 0\\ 0 & 0 & 1\end{bmatrix} \tag{14}$$

thus, **C(θ)** are given by:

$$\boldsymbol{C}(\boldsymbol{\theta})=\begin{bmatrix}C\theta_y C\theta_z & C\theta_y S\theta_z & -S\theta_y\\ C\theta_z S\theta_x S\theta_y - C\theta_x S\theta_z & C\theta_x C\theta_z + S\theta_x S\theta_y S\theta_z & C\theta_y S\theta_x\\ S\theta_x S\theta_z + C\theta_x C\theta_z C\theta_y & C\theta_x S\theta_y S\theta_z - C\theta_z S\theta_x & C\theta_x C\theta_y\end{bmatrix} \tag{15}$$

In (15), *C* and *S* stand for cosine and sine functions, respectively. According to the relevant theory about Euler angle, the derivative of the Euler angle is the rotational angular velocity of each coordinate axis of the moving frame with respect to the reference frame. Similarly, derivative of dynamic misalignment angles is used for $\boldsymbol{\omega}_{MS}^{S}$ calculation.

$$\boldsymbol{\omega}_{MS}^{S}=\begin{bmatrix}\dot{\theta}_x\\ 0\\ 0\end{bmatrix}+\boldsymbol{C}(\theta_x)\begin{bmatrix}0\\ \dot{\theta}_y\\ 0\end{bmatrix}+\boldsymbol{C}(\theta_x)\boldsymbol{C}(\theta_y)\begin{bmatrix}0\\ 0\\ \dot{\theta}_z\end{bmatrix}=\boldsymbol{M}(\boldsymbol{\theta})\dot{\boldsymbol{\theta}} \tag{16}$$

In (16), **M(θ)** is as follows:

$$\boldsymbol{M}(\boldsymbol{\theta})=\begin{bmatrix}1 & 0 & -sin(\theta_y)\\ 0 & cos(\theta_x) & cos(\theta_y)sin(\theta_x)\\ 0 & -sin(\theta_x) & cos(\theta_x)cos(\theta_y)\end{bmatrix} \tag{17}$$

Refer to (13) and (16), (12) can be rewritten as:

$$\boldsymbol{\omega}_{ib}^{S}=\boldsymbol{C}(\boldsymbol{\theta})\boldsymbol{\omega}_{ib}^{M}+\boldsymbol{M}(\boldsymbol{\theta})\dot{\boldsymbol{\theta}} \tag{18}$$

thus, angular velocity difference between the slave and the master system can be written as:

$$\boldsymbol{\omega}_{ib}^{S}-\boldsymbol{\omega}_{ib}^{M}=\boldsymbol{C}(\boldsymbol{\theta})\boldsymbol{\omega}_{ib}^{M}+\boldsymbol{M}(\boldsymbol{\theta})\dot{\boldsymbol{\theta}}-\boldsymbol{\omega}_{ib}^{M}+\cdot$$
$$\boldsymbol{\varepsilon}=\left[\boldsymbol{C}(\boldsymbol{\theta})-\boldsymbol{I}\right]\boldsymbol{\omega}_{ib}^{M}+\boldsymbol{M}(\boldsymbol{\theta})\dot{\boldsymbol{\theta}}+\boldsymbol{\varepsilon} \tag{19}$$

Accordingly, the nonlinear model of the angular velocity observation can be written as:

$$\boldsymbol{Z}_{\omega}=\left[\boldsymbol{C}(\boldsymbol{\theta})-\boldsymbol{I}\right]\boldsymbol{\omega}_{ib}^{M}+\boldsymbol{M}(\boldsymbol{\theta})\dot{\boldsymbol{\theta}}+\boldsymbol{\varepsilon}+\boldsymbol{v}_{\omega} \tag{20}$$

$\boldsymbol{v}_{w}$ is defined in (11). Note that equations (10) and (19) are equal where the dynamic misalignment angles are small.

4- 2- Angular Velocity Integral Configuration

The difference of angular velocity integral between the slave and the master system is used in this configuration.

$$\boldsymbol{I\omega}=\int_0^{\Delta t}\left(\boldsymbol{\omega}_{ib}^{n}\right)_S dt-\int_0^{\Delta t}\left(\boldsymbol{\omega}_{ib}^{n}\right)_M dt \tag{21}$$

In (21), $\boldsymbol{I\omega}$ is the difference of angular velocity integral vector between the slave and the master system. $\left(\boldsymbol{\omega}_{ib}^{n}\right)_S$ and $\left(\boldsymbol{\omega}_{ib}^{n}\right)_M$ are output of the slave and master gyroscope expressed in navigation frame and Δt indicates integral cycle, respectively. The angular velocity integral measurement model can be written as:

$$\boldsymbol{Z}_{I\omega} = \int_0^{\Delta t} \left(\boldsymbol{\omega}_{ib}^n\right)_S dt - \int_0^{\Delta t} \left(\boldsymbol{\omega}_{ib}^n\right)_M dt + \boldsymbol{v}_{I\omega} \quad ,$$

$$\boldsymbol{v}_{I\omega} \sim N(0, \boldsymbol{K}) \quad , \quad \boldsymbol{K} = \begin{bmatrix} K_N & 0 & 0 \\ 0 & K_E & 0 \\ 0 & 0 & K_N \end{bmatrix} \tag{22}$$

where, $\boldsymbol{Z}_{Iw}$ is the measurement vector constituted by the angular velocity integral and $\boldsymbol{K}$ is the associated covariance matrix. In this article, the distribution of integral of angular velocities observations is assumed Gaussian to allow the use of Kalman filters. Consider that the angular velocities measured by the gyroscopes have Gaussian distribution and this assumption is not valid in general. However, it is a conventional assumption, it will have sufficient accuracy in the desired application due to the short duration of transfer alignment. Finally, the observation vector is constituted as:

$$\boldsymbol{Z}_{6\times1} = \left[\boldsymbol{Z}_{\omega} \quad \boldsymbol{Z}_{I\omega}\right]^T \tag{23}$$

5- State Estimation Filter

Here, traditional Kalman filter and Extended Kalman Filter (EKF) are applied as the state-estimation filter in linear and nonlinear model, respectively. In order to implement the Kalman filter, the dynamics system, the measurement system, the system covariance matrix, the measurement covariance matrix and the input vector should be specified. The dynamics system is defined as:

$$\dot{\boldsymbol{X}} = \boldsymbol{F}\boldsymbol{X} + \boldsymbol{B}\boldsymbol{u} + \boldsymbol{W}_{filter} \tag{24}$$

where, $\boldsymbol{F}$, $\boldsymbol{B}$, $\boldsymbol{u}$, and $\boldsymbol{W}_{filter}$ are the system matrix, input matrix, input vector and system noise, respectively. Considering (1) to (5), these parameters can be defined as:

$$\boldsymbol{F} = \begin{bmatrix} 0_{3\times3} & \boldsymbol{I}_{3\times3} & 0_{3\times3} & 0_{3\times3} & 0_{3\times3} \\ -\boldsymbol{\beta}^2 & -2\boldsymbol{\beta} & 0_{3\times3} & 0_{3\times3} & 0_{3\times3} \\ 0_{3\times3} & 0_{3\times3} & 0_{3\times3} & 0_{3\times3} & 0_{3\times3} \\ 0_{3\times3} & 0_{3\times3} & \boldsymbol{C}_b^n & -\left[\boldsymbol{\omega}_{in}^n \times\right] & 0_{3\times3} \\ 0_{3\times3} & 0_{3\times3} & \boldsymbol{C}_b^n & \left[\boldsymbol{\omega}_{im}^n \times\right] & 0_{3\times3} \end{bmatrix} \quad , \quad \boldsymbol{\beta} = \begin{bmatrix} \beta_x & 0 & 0 \\ 0 & \beta_y & 0 \\ 0 & 0 & \beta_z \end{bmatrix} \quad , \quad \boldsymbol{B}\boldsymbol{u} = 0 \quad , \quad \boldsymbol{W}_{filter} \sim N\left(0, \boldsymbol{Q}_{filter}\right) \tag{25}$$

$\boldsymbol{Q}_{filter}$ is the covariance matrix of the dynamics system. The measurement system has linear and nonlinear model. The linear model is defined as follows:

$$\boldsymbol{Z} = \boldsymbol{H}\boldsymbol{X} + \boldsymbol{V}_{filter} \tag{26}$$

where, $\boldsymbol{H}$ stands for the measurement matrix and $\boldsymbol{V}_{filter}$ is the measurement noise. According to (11), $\boldsymbol{H}$ can be written as:

$$\boldsymbol{H}_{6\times15} = \begin{bmatrix} \left[\boldsymbol{\omega}_{ib}^M \times\right] & \boldsymbol{I}_{3\times3} & \boldsymbol{I}_{3\times3} & \boldsymbol{0}_{3\times3} & \boldsymbol{0}_{3\times3} \\ \boldsymbol{0}_{3\times3} & \boldsymbol{0}_{3\times3} & \boldsymbol{0}_{3\times3} & \boldsymbol{0}_{3\times3} & \boldsymbol{I}_{3\times3} \end{bmatrix} \quad , \quad \boldsymbol{V}_{filter} \sim N\left(0, \boldsymbol{R}_{filter}\right) \tag{27}$$

$\boldsymbol{R}_{filter}$ is the measurement covariance matrix. The nonlinear mode of the measurement model is defined as:

$$\boldsymbol{Z} = h(\boldsymbol{X}) + \boldsymbol{V}_{filter} \tag{28}$$

where $h(\boldsymbol{X})$ can be computed by (20), and $\boldsymbol{V}_{filter}$ is defined in (27). The EKF equations for nonlinear model are as follows [22]:

- **Prediction phase**:

$\hat{\boldsymbol{X}}_{k\|k-1} = \mathbf{F}_k \hat{\boldsymbol{X}}_{k-1\|k-1}$	Predicted state estimate
$\mathbf{P}_{k\|k-1} = \mathbf{F}_k \mathbf{Q}_{k-1\|k-1} \mathbf{F}_k^{\mathrm{T}} + \mathbf{Q}_k$	Predicted covariance estimate

- **Update phase**:

$\tilde{\mathbf{y}}_k = \mathbf{Z}_k - \mathrm{h}\left(\hat{\mathbf{X}}_{k\|k-1}\right)$	Innovation or measurement residual
$\mathbf{S}_k = \mathbf{H}_k \mathbf{P}_{k\|k-1} \mathbf{H}_k^{\mathrm{T}} + \mathbf{R}_k$	Innovation (or residual) covariance
$\mathbf{K}_k = \mathbf{P}_{k\|k-1} \mathbf{H}_k^{\mathrm{T}} \mathbf{S}_k^{-1}$	Kalman gain
$\hat{\mathbf{X}}_{k\|k} = \hat{\mathbf{X}}_{k\|k-1} + \mathbf{K}_k \tilde{\mathbf{y}}_k$	Update state estimate
$\mathbf{P}_{k\|k} = (\mathbf{I} - \mathbf{K}_k \mathbf{H}_k) \mathbf{P}_{k\|k-1}$	Update covariance estimate

where $\boldsymbol{H}$ matrix for EKF can be calculated as follows:

$$\mathbf{H}_k = \left.\frac{\partial \mathrm{h}(\mathrm{X})}{\partial \mathbf{X}}\right|_{\hat{\mathbf{X}}_{k|k-1}} \tag{29}$$

In extended Kalman filtering, the linearization is done around the last predicted of the state. Therefore, in (29), $\hat{\mathbf{X}}_{k|k-1}$ is the last predicted of the state.

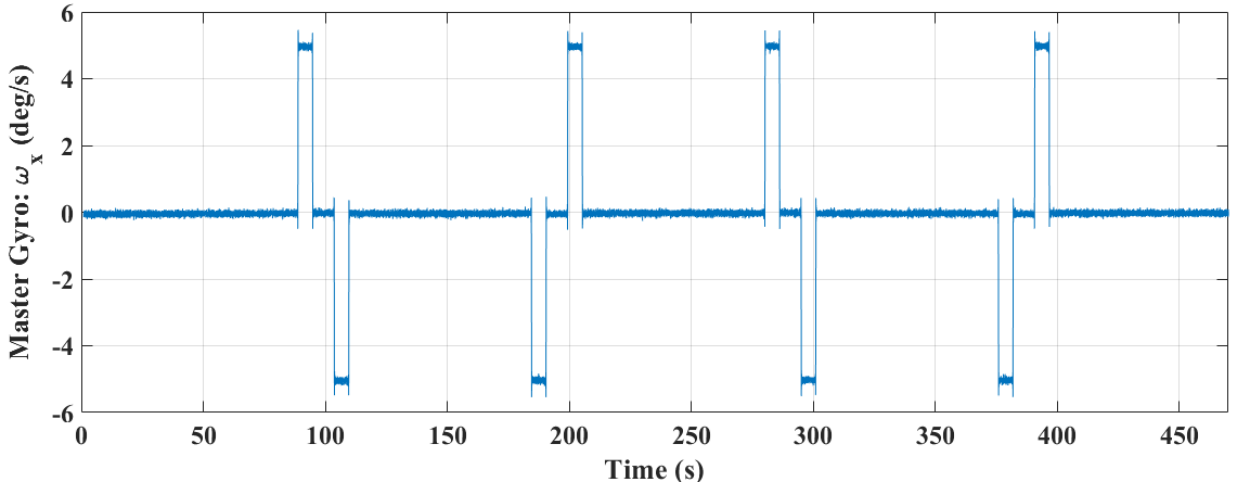

Fig. 3. Output data of the master gyroscope in the x direction

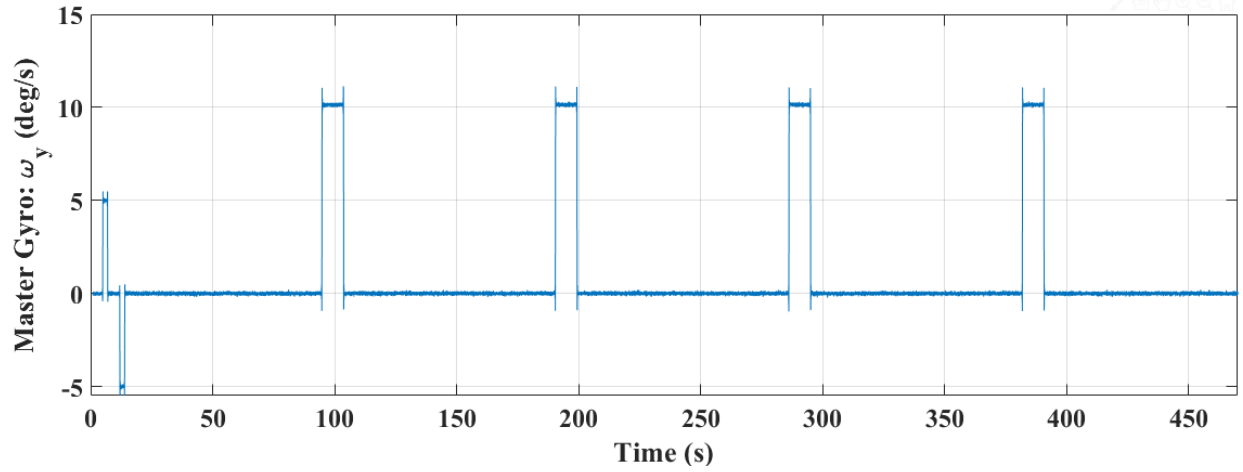

Fig. 4. Output data of the master gyroscope in the y direction

6- Simulation Results

Several simulated tests have been carried out to assess the accuracy and the performance of the proposed transfer alignment configuration. First, the main simulation parameters are described and then the results are discussed. In the simulation, the system and measurement covariance matrices are defined as $\boldsymbol{Q}_{filter} = 0.5\times\boldsymbol{I}_{15\times15}$ and $\boldsymbol{R}_{filter} = 0.01\times\boldsymbol{I}_{6\times6}$, respectively. Initial values of the state vector and the estimation covariance matrix are considered as $\boldsymbol{X}_0 = [0_{9\times1} \quad [10 \;\; 30 \;\; 20] \quad [5 \;\; 7 \;\; 8]]^T$, $\boldsymbol{P}_0 = 0.5\times\boldsymbol{I}_{15\times15}$, respectively. Slave gyroscope biases are considered 0.6, 0.5 and 0.4 degree per second. The output data of master gyroscope around x, y, and z-axis are illustrated in Fig. 3, Fig. 4, and Fig. 5, respectively [22].

Simulation results of the dynamic misalignment angles are illustrated in Fig. 6 to Fig. 8. According to the results, the estimations cannot track the real values of the dynamic misalignment angles, exactly. Low degree of observability can be one of the main reasons to poor estimation of the dynamic misalignment angles. However, the change rate of real values is low and the estimations are satisfied.

Simulation results of the slave gyroscope biases are illustrated in Fig. 9 to Fig. 11. It can be inferred from the results that bias estimation in x and y-axis have more dynamics compared to z-axis. This is due to the effect that dynamic misalignment angles derivation on the slave gyroscope biases in x and y-axis. It can be also inferred from (10). The derivation of dynamic misalignment angle vector and the slave gyroscope bias vector are explicitly appeared in the linear model of the angular velocity configuration. Therefore, more derivation of the dynamic misalignment angle leads to more variation in the gyroscope bias estimation. Additionally, this can be proved by nonlinear model of the angular velocity configuration explained in (19).

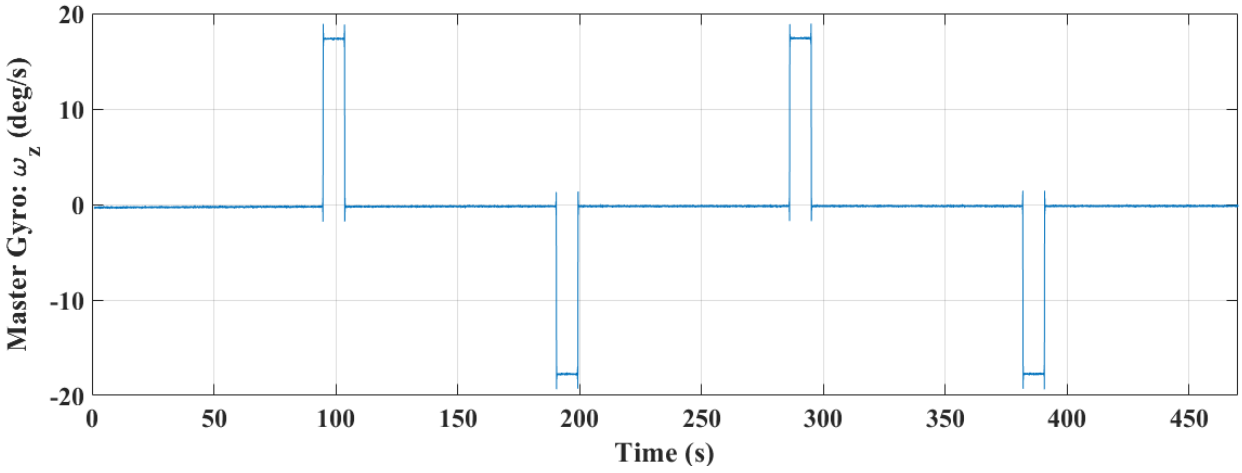

Fig. 5. Output data of the master gyroscope in the z direction

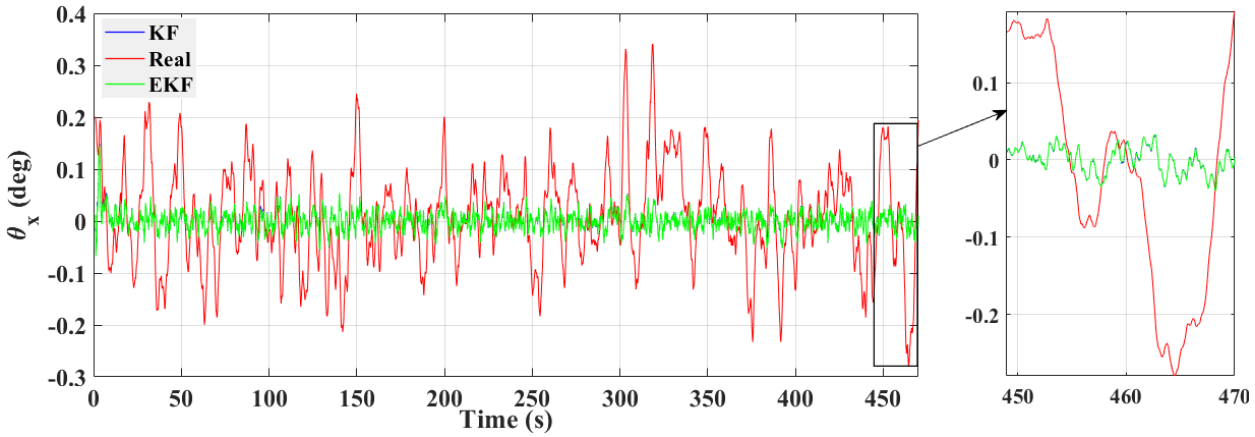

Fig. 6. Simulation result of the dynamic misalignment angle in the x direction

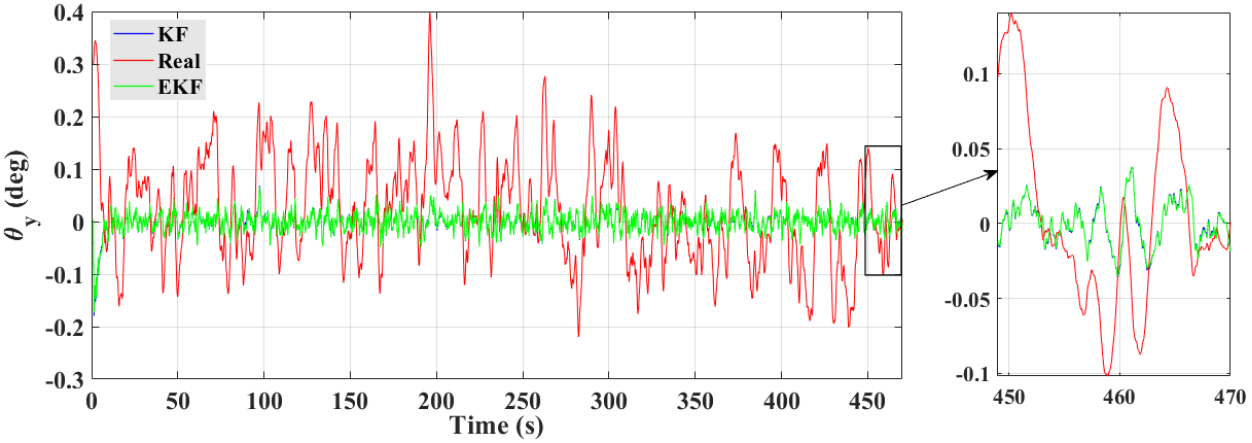

Fig. 7. Simulation result of the dynamic misalignment angle in the y direction

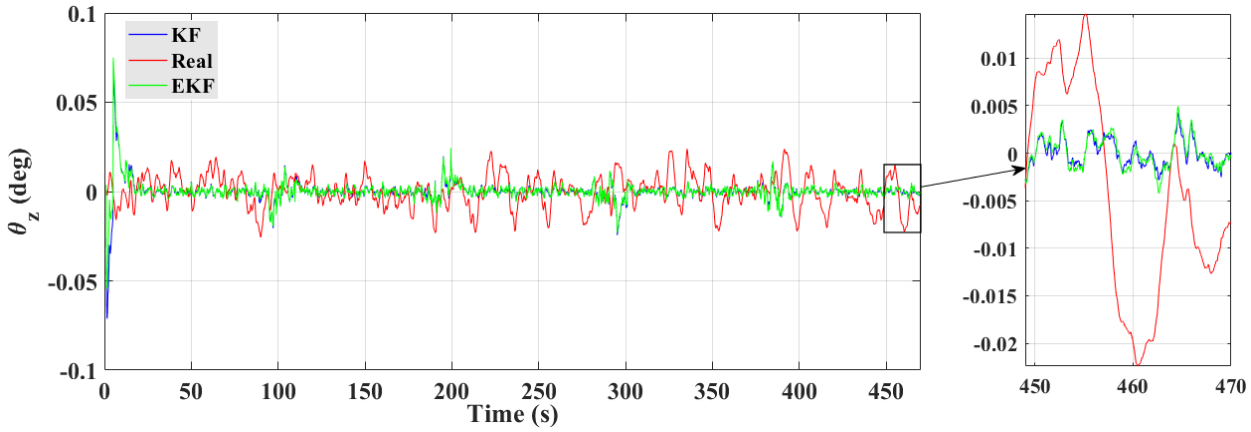

Fig. 8. Simulation result of the dynamic misalignment angle in the z direction

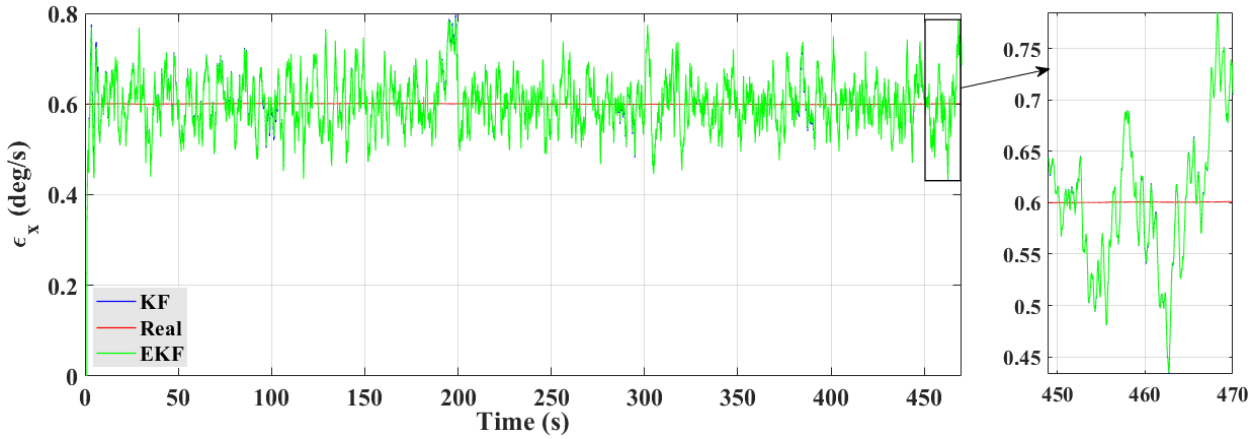

Fig. 9. Simulation results of the slave gyroscope bias in the x direction

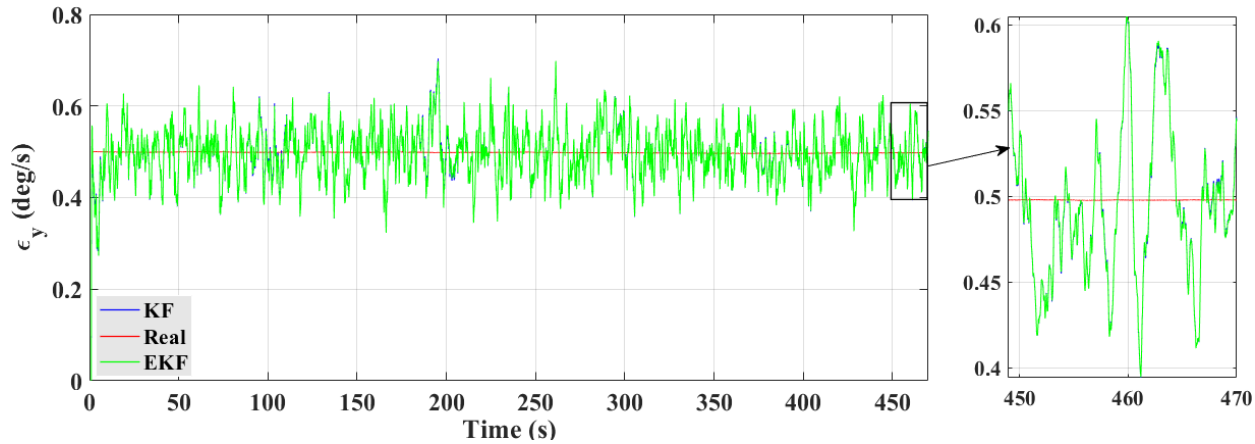

Fig. 10. Simulation results of the slave gyroscope bias in the y direction

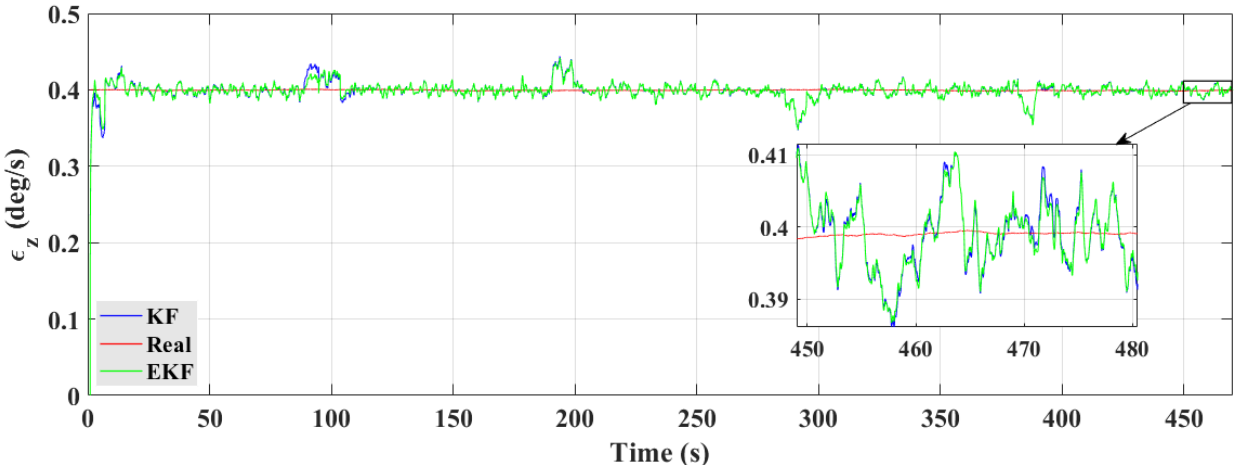

Fig. 11. Simulation results of the slave gyroscope bias in the z direction

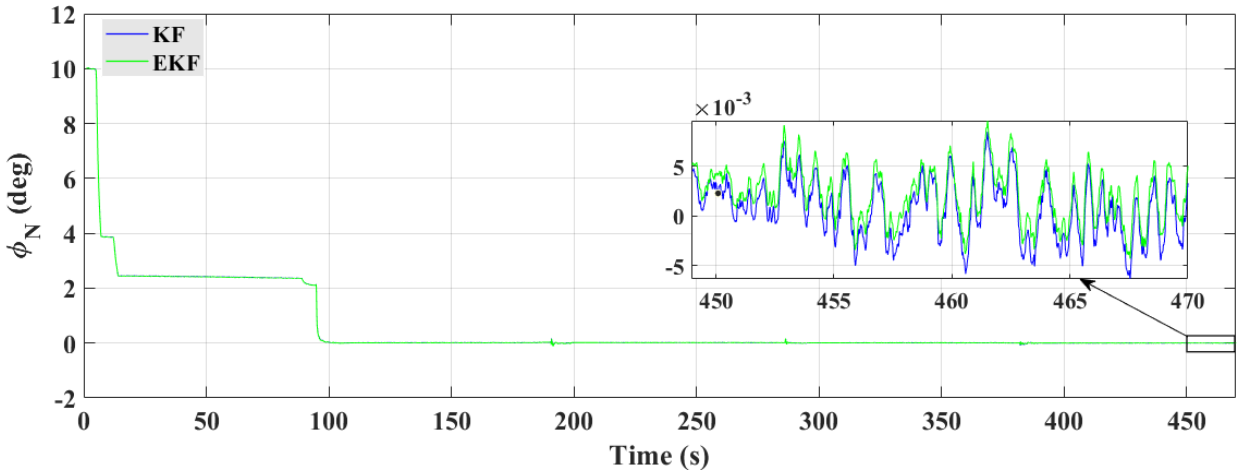

Fig. 12. Simulation results of the orientation error in the North direction

Simulation results of the slave orientation error are illustrated in Fig. 12 to Fig. 14. According to the results, the orientation error estimation is converged to zero. Comparing output of the master gyroscope (Fig. 3 to Fig. 5) and orientation error simulation (Fig. 12 to Fig. 14), a jump in the master gyroscope leads to better estimation convergence in the orientation error. In other words, higher maneuvering brings about rich data for better estimation of the orientation error. Accordingly, with master system maneuvering, better observation of the orientation error will be acquired. Based on Fig. 12 to Fig. 14, almost 200 seconds are necessary for the alignment convergence with these maneuvers.

The residual signal of the state estimation filter for both KF and EKF are shown in Fig. 15 and Fig. 16. Left figures illustrate the residual signals corresponding to the angular velocity measurements and right figures illustrate the residual signals corresponding to the angular velocity integral.

The residual signal of the angular velocity in x and y-axis have more dynamics compared to z-axis. This is due to the difference between derivation of the dynamic misalignment angle model and the predicted values in x and y-axis. According to the results, the residual signals converge to zero and appropriate performance of the state estimation is satisfied. For better evaluation, the RMSE of the estimated states are gathered in Table 1.

According to Table 1, RMSE of the state estimation is approximately equal for both KF and EKF. Considering the results of simulation, the performance of linear and nonlinear method is similar, approximately and this is due to the small values of the misalignment angles. Additionally, a Monte-Carlo simulation is applied for 200 consecutive runs and the RMS error of estimation is gathered in Table 2.

According to Table2, the RMSE of KF and EKF is equal after 200 runs and this is due to small misalignment angles. In other words, the small nonlinearity of the nonlinear model causes the performance of linear and nonlinear model be the same.

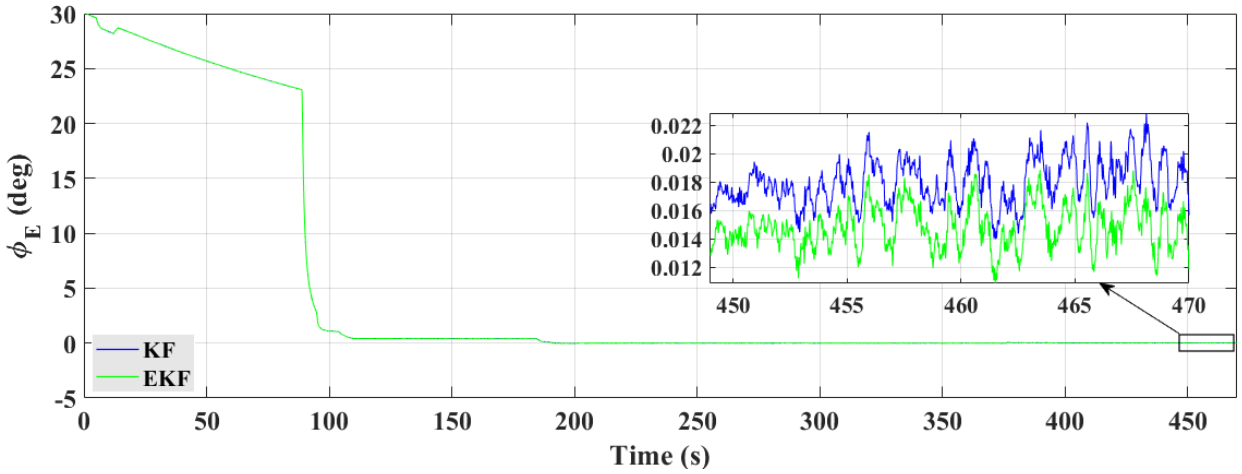

Fig. 13. Simulation results of the orientation error in the East direction

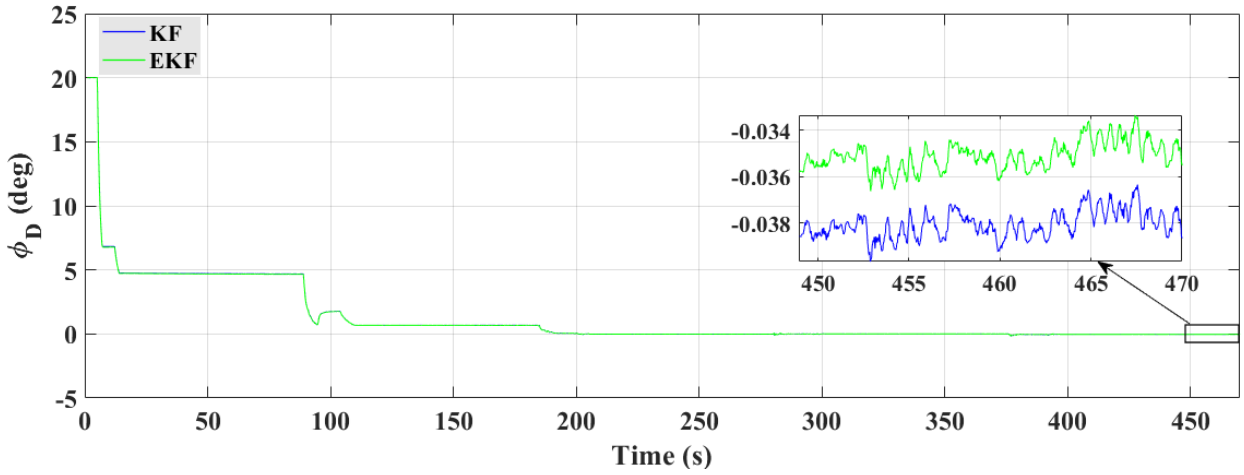

Fig. 14. Simulation results of the orientation error in the Down direction

Table 1. RMSE of the estimated states

	KF	EKF
Slave gyroscope bias in x direction (deg/s)	0.058264	0.058265
Slave gyroscope bias in y direction (deg/s)	0.05497	0.054896
Slave gyroscope bias in z direction (deg/s)	0.0094581	0.0086428
Dynamic misalignment angle in x direction (deg)	0.10412	0.10403
Dynamic misalignment angle in y direction (deg)	0.087839	0.087743
Dynamic misalignment angle in z direction (deg)	0.011289	0.011134

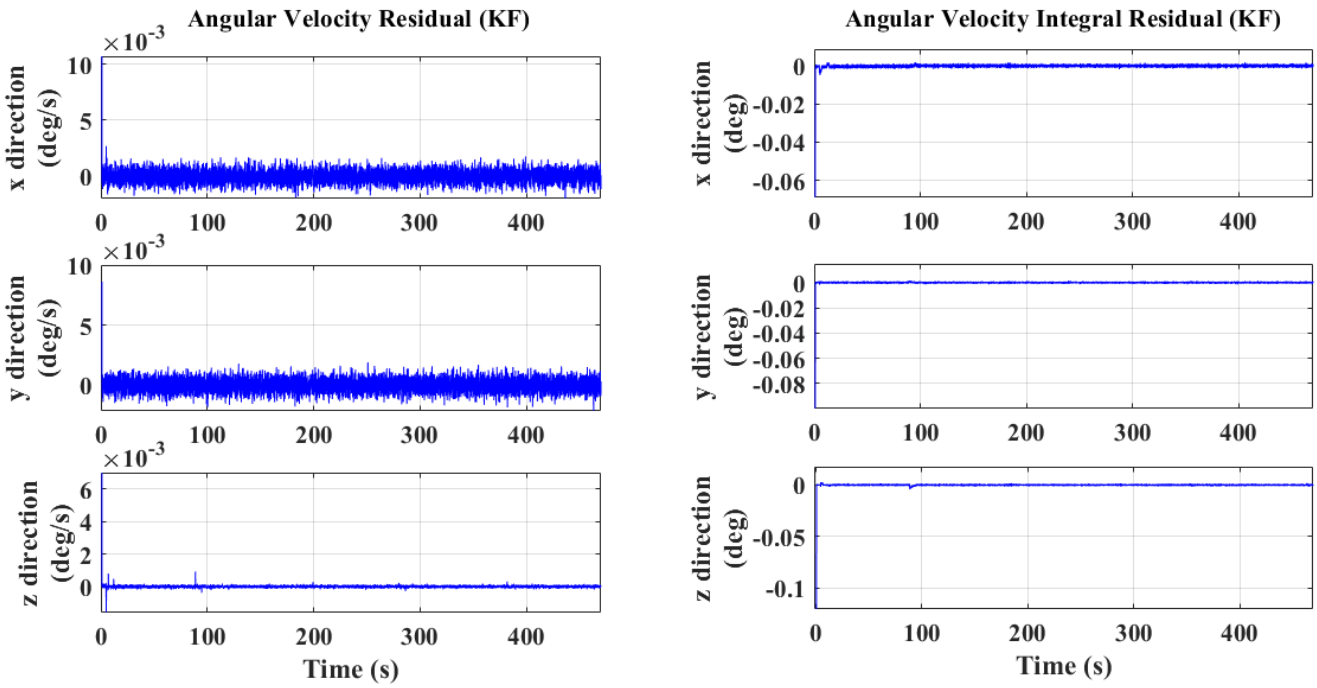

Fig. 15. Residual signals of the linear configuration

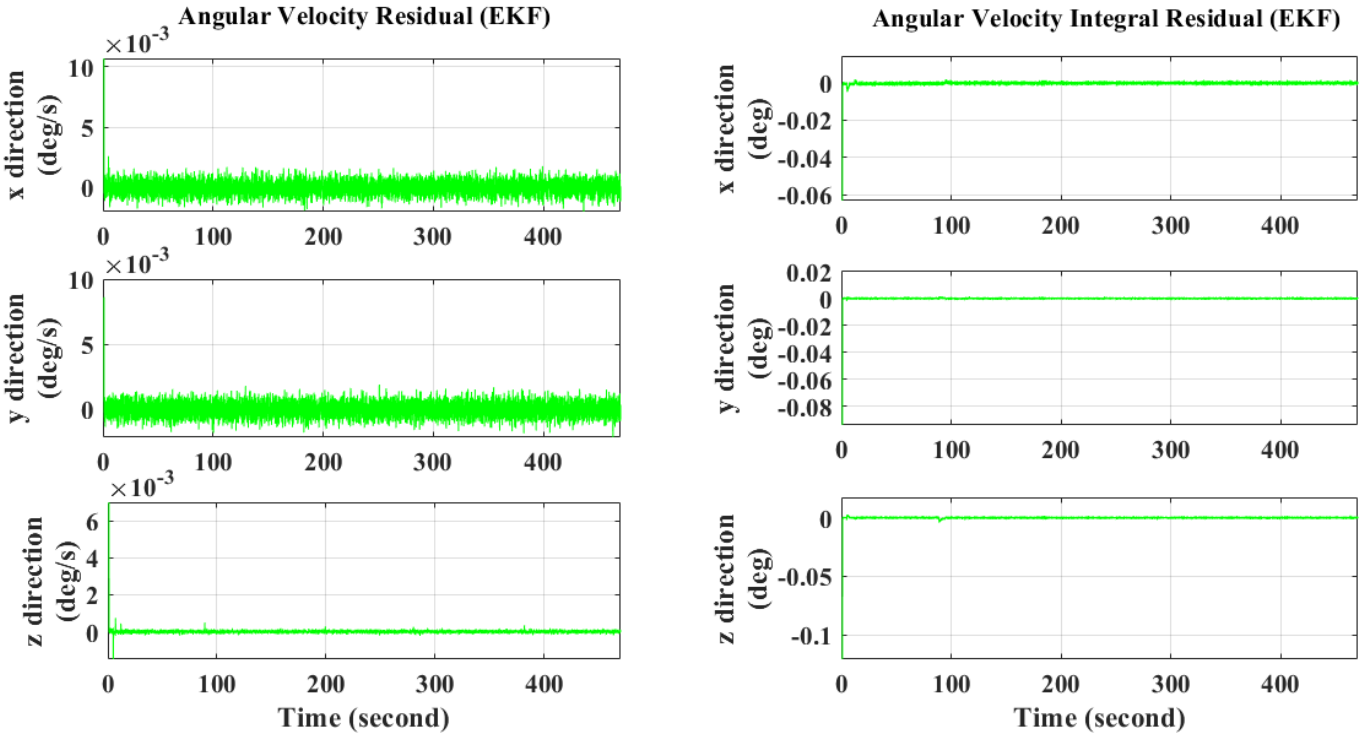

Fig. 16. Residual signals of the nonlinear configuration

Table 2. RMSE of 200 runs Monte-Carlo simulation

	KF	EKF
Slave gyroscope bias in x direction (deg/s)	0.0531	0.0531
Slave gyroscope bias in y direction (deg/s)	0.0532	0.0532
Slave gyroscope bias in z direction (deg/s)	0.0075	0.0075
Dynamic misalignment angle in x direction (deg)	0.0965	0.0965
Dynamic misalignment angle in y direction (deg)	0.0210	0.0210
Dynamic misalignment angle in z direction (deg)	0.0117	0.0117
Derivation of dynamic misalignment angle in x direction (deg/s)	0.0589	0.0589
Derivation of dynamic misalignment angle in y direction (deg/s)	0.0590	0.0590
Derivation of dynamic misalignment angle in z direction (deg/s)	0.0064	0.0064

7- Conclusion

This paper deals with design and simulation of transfer alignment algorithm at sea based on the angular velocity and angular velocity integral configuration. Where there are no auxiliary sensors for position and velocity computation and also the initial navigation data are not available, the necessity of the proposed transfer alignment algorithm is considerably increased. The proposed method has been developed for estimation of misalignment angle, orientation errors and slave gyroscope bias. Linear and nonlinear models were used, and their performance has been investigated for transfer alignment configuration. According to the simulation results, both the linear and nonlinear models lead to similar performance for small values of the misalignment angles. We have seen higher maneuvering brings about rich data for better estimation of the orientation errors. Moreover, the derivation of the dynamic misalignment angle impresses the slave gyroscope bias. It makes more variation in the slave gyroscope bias estimation. Low degree of observation was the main reason to poor estimation of dynamic misalignment angles. Additionally, a Monte-Carlo simulation developed based on the 200 consecutive runs and the RMS error of the estimations presented. We have seen the performance of linear and nonlinear model was the same due to small misalignment angles. Although, we didn't perform observability analysis in this research, adding acceleration integral to angular velocity and angular velocity integral measurements can lead to better dynamic misalignment angles estimation. These are proposed for related future researches.

References

[1] Xiaorong, S. and S. Yongzhu. Angular rate matching method for shipboard transfer alignment based on H∞ filter. in 2011 6th IEEE Conference on Industrial Electronics and Applications. 2011. IEEE.

[2] Song, L., Z. Duan, and J. Sun, Application of Filter on the Angular Rate Matching in the Transfer Alignment. Discrete Dynamics in Nature and Society, 2016.

[3] Majeed, S. and J. Fang. Performance improvement of angular rate matching shipboard transfer alignment. in 2009 9th International Conference on Electronic Measurement & Instruments. 2009. IEEE.

[4] Amuei. M., Dehghan. S.M.M., Nourmohammadi. H., Design and simulation of transfer alignment algorithm at sea with angular velocity configuration. in 10th Majlesi Conference on Electrical Engineering. 2021. (in Persian)

[5] Liu, X., et al. Ship-borne transfer alignment under low maneuver. in Applied Mechanics and Materials. 2012. Trans Tech Publ.

[6] Geng, C., et al. Real-time Estimation of Dynamic Lever Arm Effect of Transfer Alignment for Wing's Elastic Deformation. in 2018 IEEE/ION Position, Location and Navigation Symposium (PLANS). 2018.

[7] Cao, Q., M. Zhong, and J. Guo, Non-linear estimation of the flexural lever arm for transfer alignment of airborne distributed position and orientation system. IET Radar, Sonar & Navigation, 2017. 11(1): p. 41-51.

[8] Liu, X., et al. Rapid alignment method of INS with large initial azimuth uncertainty under complex dynamic disturbances. in Proceedings of 2012 UKACC

International Conference on Control. 2012. IEEE.

[9] Song, L., et al. Application of Federated and Fuzzy Adaptive Filter on the Velocity and Angular Rate Matching in the Transfer Alignment. in International Conference on Intelligent Robotics and Applications. 2015. Springer.

[10] Yong-Jun, W., X. Jing-Shuo, and Y. Tao. Application of velocity plus fixed axial angular velocity match method in transfer alignment of SINS based on the moving base. in 2021 4th International Conference on Advanced Electronic Materials, Computers and Software Engineering (AEMCSE). 2021. IEEE.

[11] Chen, Weina, et al. Adaptive transfer alignment method based on the observability analysis for airborne pod strapdown Inertial Navigation System. Scientific Reports 12.1 (2022): 1-14.

[12] Yuksel, Y. Design and analysis of transfer alignment algorithm. Middle East Technical University, MS Thesis (2005).

[13] Yang, Ping, Xiyuan Chen, and Junwei Wang. Decoupling of airborne dynamic bending deformation angle and its application in the high-accuracy transfer alignment process. Sensors 19.1 (2019): 214.

[14] Nourmohammadi, H. and J. Keighobadi, Decentralized INS/GNSS system with MEMS-grade inertial sensors using QR-factorized CKF. IEEE Sensors Journal, 17 (11) (2017) p. 3278-3287.

[15] Chattaraj, S., A. Mukherjee, and S. Chaudhuri, Transfer alignment problem: Algorithms and design issues. Gyroscopy and navigation, 4 (3) (2013) p. 130-146.

[16] Gong, X. and L. Chen, A conditional cubature Kalman filter and its application to transfer alignment of distributed position and orientation system. Aerospace Science and Technology, 95 (2019) p. 105405.

[17] Rahimi, H., A.A. Nikkhah, and K. Hooshmandi, A fast alignment of marine strapdown Inertial Navigation System based on adaptive unscented Kalman Filter. Transactions of the Institute of Measurement and Control, 43 (4) (2021) p. 749-758.

[18] Xu, G., et al., A Computationally Efficient Variational Adaptive Kalman Filter for Transfer Alignment. IEEE Sensors Journal, 20 (22) (2020) p. 13682-13693.

[19] Milanchian, H., J. Keighobadi, and H. Nourmohammadi, Magnetic calibration of three-axis strapdown magnetometers for applications in MEMS attitude-heading reference systems. AUT Journal of Modeling and Simulation, 47 (1) (2015) p. 55-65.

[20] Wang, Y., et al. Research of transfer alignment for airborne distributed inertial attitude measurement system. in 3rd International Conference on Electric and Electronics. 2013. Atlantis Press.

[21] Nourmohammadi, H. and J. Keighobadi, Integration scheme for SINS/GPS system based on vertical channel decomposition and in-motion alignment. AUT Journal of Modeling and Simulation, 50 (1) (2018) p. 13-22.

[22] Gonzalez, R., J.I. Giribet, and H.D. Patino, NaveGo: A simulation framework for low-cost integrated navigation systems. Journal of Control Engineering and Applied Informatics, 17 (2) (2015) p. 110-120.

HOW TO CITE THIS ARTICLE

M. Amuei, S. M. Mehdi Dehghan, H. Nourmohammadi, M. A. AlirezaPouri,Transfer Alignment Configuration Based on Angular Velocity and Angular Velocity Integral Applied to Marine Vehicles, Title. AUT J. Model. Simul., 54(1) (2022) 31-44.

DOI: 10.22060/miscj.2022.21010.5268